Pd–assisted growth of InAs nanowires

S. Heun,[*,†] B. Radha,[‡] D. Ercolani,[†] G. U. Kulkarni,[‡] F. Rossi,[¶] V. Grillo,[§,¶]

G. Salviati,[¶] F. Beltram,[†] and L. Sorba[†]

NEST, CNR–INFM and Scuola Normale Superiore, Piazza S. Silvestro 12, I–56127 Pisa, Italy, Jawaharlal Nehru Centre for Advanced Scientific Research, Jakkur P. O., Bangalore 560 064, India, IMEM–CNR, Parco Area delle Scienze 37/A, I–43010 Parma, Italy, and INFM–CNR National Research Center on nanoStructures and bioSystems at Surfaces (S3), via Campi 213/A, I–41100, Modena (Italy)

E-mail: stefan.heun@sns.it

Abstract

We report the Pd–assisted chemical beam epitaxy growth of zincblende InAs nanowires. Pd–assisted InAs nanowires are grown on InAs$(1\,1\,1)$A substrates by employing Pd octane– and hexadecyl–thiolates as catalyst precursors. The structural properties of Pd–assisted InAs nanowires are investigated by scanning and transmission electron microscopy. Furthermore, we demostrate the growth of InAs nanowires on patterned substrates by employing the Pd hexadecylthiolate precursors as a direct–write resist in electron beam lithography.

[*]To whom correspondence should be addressed

[†]NEST, CNR–INFM and Scuola Normale Superiore, Piazza S. Silvestro 12, I–56127 Pisa, Italy

[‡]Jawaharlal Nehru Centre for Advanced Scientific Research, Jakkur P. O., Bangalore 560 064, India

[¶]IMEM–CNR, Parco Area delle Scienze 37/A, I–43010 Parma, Italy

[§]INFM–CNR National Research Center on nanoStructures and bioSystems at Surfaces (S3), via Campi 213/A, I–41100, Modena (Italy)

Catalyst–assisted growth of semiconductor nanowires (NW) has been intensively studied for the last decade.[1] The sythesis of NWs often involves the vapor–liquid–solid (VLS) or vapor–solid–solid (VSS) mechanisms, in which a metal nanoparticle catalyzes the growth. NWs have a high potential for electronic, optoelectronic, and sensor applications.[2,3] The commonly used catalyst material for NW growth is Au,[4] because it is chemically inert and thermally stable. Also several other materials have been explored for their use as catalyst for NW growth.[5–8] A very attractive candidate is Pd, because it allows for good ohmic contacts to semiconductors,[9–12] has a high molecular connectivity useful for bio–sensing,[13] and shows a high hydrogen response which might be exploited in sensors.[14] While Pd has been used to grow metallic NW,[15] Si NW,[16] SnO_2 NWs,[5] and carbon nanotubes,[17,18] to our knowledge it has never been used to grow III–V NWs. Here, we demonstrate for the first time Pd–assisted growth of zincblende InAs NWs.

With respect to other catalyst materials, Pd offers the advantage that nanoparticles can be obtained from precursors which are direct–write electron resists. This allows for a patterning of the nanoparticle film without additional processing steps. Following this idea we demonstrate the selctive growth of InAs NWs on a patterned Pd precursor film.

The Pd catalyst nanoparticles for the nanowire growth were obtained from Pd octanethiolate [$Pd(SC_8H_{17})_2$, short PdC8] and Pd hexadecylthiolate [$Pd(SC_{16}H_{33})_2$, short PdC16] precursors. The procedure adopted for the synthesis of the precursors is given elsewhere.[19] The precursor solution was spin–coated at 2000 rpm as a smooth film of a few nanometers thickness. Next, thermolysis was carried out in air at 300°C for 30 min which yielded $5-15$ nm sized Pd–catalyst particles.[20,21]

InAs nanowires (NWs) were grown by chemical beam epitaxy (CBE) in a Riber Compact–21 system. The system employs pressure control of the metalorganic (MO) precursors in the lines to vary their fluxes on the sample during growth. The precursors used for the NW growth are trimethylindium (TMI) and tertiarybutylarsine (TBA). Details of the growth setup can be found elsewhere.[22] The Pd–catalyst–deposited InAs substrates were transferred to the CBE system where they were heated under TBA flow for 20 min at 505°C in order to remove the InAs surface oxide.

In order to monitor the Pd nanoparticle size after this annealing step, one sample was removed from the chamber before NW growth, and measured by scanning electron microscopy (SEM) on a Zeiss Ultra Plus field–emission SEM. The average Pd particle density is measured to be $16 \pm 2\ \mu\text{m}^{-2}$. The histogram of the particle area distribution is well described by an exponential curve $f(x) = A\exp(-x/\tau)$, with $\tau = 950\ \text{nm}^2$, a value which corresponds to a particle diameter of 35 nm. This indicates that significant aggregation of nanoparticles occured during substrate deoxidation.

We explored the growth of InAs NWs on InAs substrates of different orientations: (100), (111)A (In–terminated), and $\left(\bar{1}\bar{1}\bar{1}\right)$B (As–terminated). Figure 1 shows images of Pd–assisted NW growth on InAs(100) substrates. The images were obtained by SEM with an accelerating voltage of 5 kV. NWs do not grow perpendicular to the surface, but along the $\langle 011 \rangle$ directions under an angle of $55.5 \pm 2.3^\circ$ to the normal, which corresponds to the different $\langle 111 \rangle$ directions. The majority of the wires (approximately 85%) grow in the $[111]$A or $\left[1\bar{1}\bar{1}\right]$A directions, while the remaining wires grow in the $\left[1\bar{1}1\right]$B or $\left[11\bar{1}\right]$B directions. Even on the $\{011\}$ cleavage faces of the (100) wafer, the wires grow mainly in $\langle 111 \rangle$A directions.

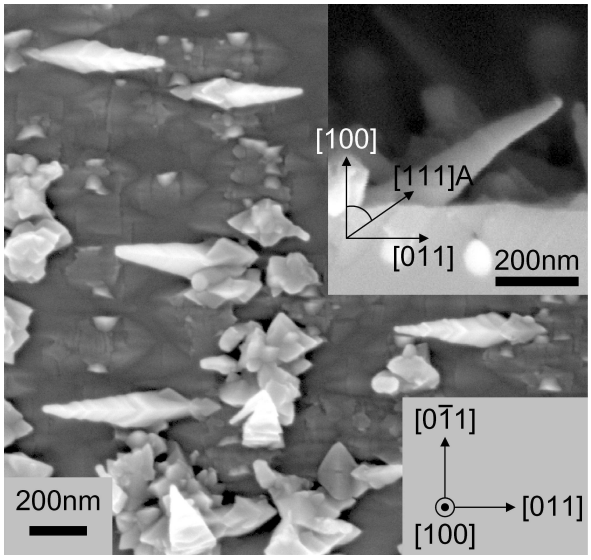

Figure 1: Plan–view SEM micrograph of Pd–assisted InAs NWs grown on an InAs(100) substrate. The inset shows a cross–sectional view. The NWs are preferentially oriented along the $\langle 111 \rangle$A directions of the substrate, including an angle of approximately 55° with the surface normal.

Few wires grow on the InAs$\left(\bar{1}\bar{1}\bar{1}\right)$B surface. We observed mainly pyramidal island growth at Pd nanoparticle locations (see Figure 2(b)). This is somewhat surprising, as for III–V NWs the preferential growth direction is usually a $\langle\bar{1}\bar{1}\bar{1}\rangle$B direction.[23]

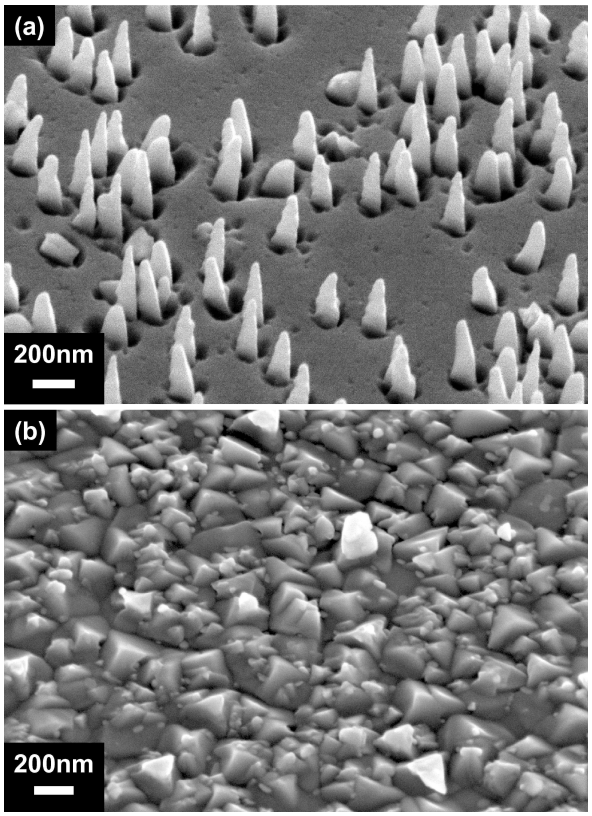

Figure 2: SEM micrographs of Pd–assisted InAs NWs grown on (a) InAs$(1\,1\,1)$A and (b) InAs$\left(\bar{1}\bar{1}\bar{1}\right)$B substrates. For the SEM measurements, the samples were tilted by an angle of 45°.

Best results were obtained for growth on the InAs$(1\,1\,1)$A surface. NWs oriented along the $[1\,1\,1]$A direction are clearly visible in the SEM image in Figure 2(a). No NWs growing in other directions were observed. The NW density is 14 ± 2 μm^{-2}. This number corresponds within error bars to the density of Pd particles before growth, so that we conclude that on average each Pd particle leads to the nucleation and growth of one NW. Before NW growth, the InAs$(1\,1\,1)$A surface displayed a 2×2 reconstruction in reflection high energy electron diffraction (RHEED), in agreement with previous reports.[24] The RHEED pattern observed after NW growth indicates epitaxial growth of the NWs in $[1\,1\,1]$A direction with zincblende structure (see the Supporting

Information for more details).

Optimization of the growth procedure was performed by changing the substrate temperature in the range of $300 - 360^{\circ}$C, TBA flow in the pressure range of $1.0 - 3.0$ Torr and TMI flow in the pressure range of $0.1 - 0.45$ Torr. Optimised InAs NWs were grown for 1 to 4 hours at a temperature of 330°C, with MO line pressures of 0.45 and 2.0 Torr for TMI and TBA, respectively. Identical results were obtained for growth with PdC8 and PdC16 precursors. Remarkably, good quality NWs could only be obtained in a small temperature window of $\pm 20^{\circ}$C around the optimal growth temperature.

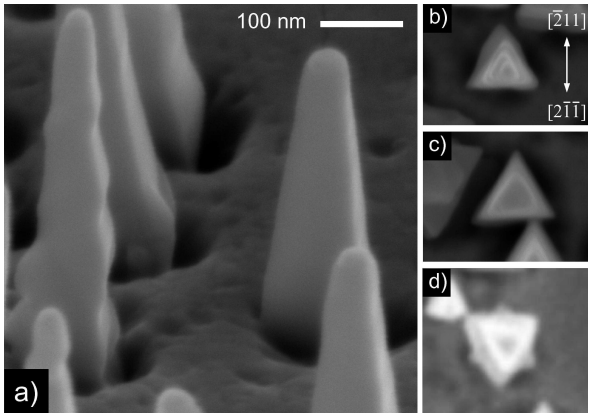

Figure 3: High–resolution SEM images of Pd–assisted InAs NWs on InAs$(1\,1\,1)$A. (a) Side–view; the substrate was tilted by 45°. The image shows NWs with smooth and zig–zag sidewalls. (b) Top–view SEM image of a NW with zig–zag sidewalls. (c) Same for a NW with smooth sidewalls. (d) NW with a twinning defect. The crystallographic directions given in (b) are valid for (b) – (d).

High–resolution SEM (HRSEM) images reveal details of the morphology of the NWs grown on InAs$(1\,1\,1)$A. Figure 3(a) shows two types of NWs: those with smooth sidewalls, and those with zig–zagged sidewalls. Figure 4 shows size histograms for two different growth temperatures (330°C and 340°C) obtained from SEM analyses, by measuring the near–tip NW diameter in a number of HRSEM images. For growth temperatures lower than 330°C, NWs tend to be more and more defective so that an unambiguous classification as zig–zag or smooth becomes increasingly difficult. As shown in Figure 4, a bimodal size distribution is observed which can be well fitted with two Gaussian curves: for the NWs grown at 330°C, the zig–zag NWs have a size at the tip of 24 ± 5 nm, while for the NWs with smooth sidewalls, the value is 40 ± 9 nm. These values are

independent of growth time in an interval from 2 to 4 hours, i.e. for both types of NW a change of tip diameter with growth time is not observed. At the cross–over of the two Gaussian curves, a critical tip diameter d_c (about 30 nm at 330°C and 48 nm at 340°C, see arrows in Figure 4) can be identified. A correlation between the sidewall morphology and the NW tip diameter can be hypothesized: when the tip diameter is larger than the critical diameter, the NWs grow with smooth sidewalls. On the contrary, when the tip diameter is noticeably lower than d_c, we observe the growth of a zig–zagged NW. Figure 4 shows also that for a higher growth temperature, a different distribution is obtained, with a larger relative number of zig–zag NWs and with average values of the distributions shifted to higher values. The insets of Figure 4 show the cumulative NW tip size distributions, which were obtained by adding the distributions of zig–zagged and smooth NWs. The cumulative histograms for the two growth temperatures are rather similar, which implies that apart from the variations in the relative numbers of zig–zag and smooth NWs, the two growth temperatures yield virtually identical results.

The average height of the NWs after 2 and 4 hours of growth is 420 ± 80 nm and 930 ± 190 nm, respectively, independent of the type of NW. The average growth rate calculated from these numbers is 3.5 ± 0.7 nm/min and 3.9 ± 0.8 nm/min, respectively. Therefore, the growth rate is constant (within experimental uncertainty) and independent of NW type, height, or tip diameter. Furthermore, Figure 3(a) shows that the NW are tapered, with a smaller diameter at the top. In contrast to the constant tip width, the base width of the NWs increases with growth time. For the NWs with smooth sidewalls, the base width histogram fitted with a Gaussian curve gives an average value of 136 nm and a width of 15 nm after 2 hours of growth and 190 nm and 21 nm, respectively, after 4 hours of growth. Similar values are obtained for the NWs with zig–zag sidewalls. This shows that the tapering of the NWs is related to the growth of additional material on the sidewalls of the NWs during growth. Considering the average tip width, the lateral growth rates are estimated to be less than 0.7 nm/min, i.e. less than $1/5$ of the growth rate in axial direction. The cone–like shape of the NWs allows interesting applications in photovoltaics, where nanocones are shown to be both efficient absorbers and antireflection layers.[25]

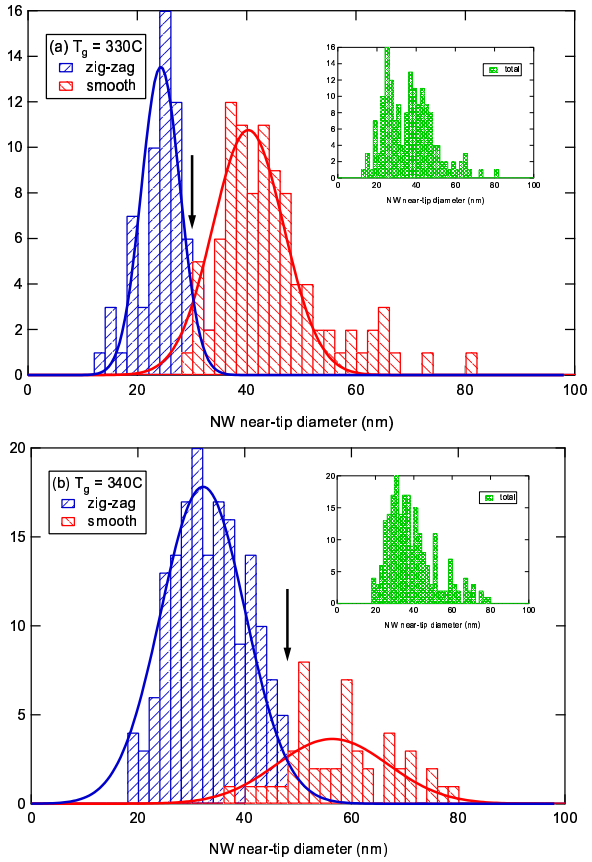

Figure 4: Histograms of the near–tip size distribution for the two sets of NWs, with zig–zagged or smooth sidewalls. The arrows indicate the critical tip diameter d_c. Growth temperature T_g: (a) 330°C, (b) 340°C. The average diameters are (a) for zig–zag 24 ± 5 nm, for smooth 40 ± 9 nm, (b) for zig–zag 32 ± 11 nm, for smooth 57 ± 11 nm. Critical diameter d_c in (a) 30 nm, in (b) 48 nm. The insets show the respective cumulative histograms (= zig–zag + smooth).

Top–view SEM pictures (Figure 3(b) and (c)) reveal furthermore that both types of NWs have a triangular cross–section. A statistical analysis of several top–view SEM images shows that almost all triangles point in the $[\bar{2}11]$ direction, both for NWs with smooth and zig–zag sidewalls. This indicates that there are three major side facets perpendicular to the growth direction: $(2\bar{1}\bar{1})$, $(\bar{1}\bar{1}2)$, and $(\bar{1}2\bar{1})$, which all belong to the $\{112\}$A surfaces and are terminated in the group III element In.[26] Triangular NWs were also reported.[23,26,27]

High–resolution SEM images of some of the few triangles which point in the opposite $[2\bar{1}\bar{1}]$ direction (see Figure 3(d)) suggest that these NWs initially grow like the others with a triangular base pointing in the $[\bar{2}11]$ direction, and then, most likely due to insertion of a rotational stacking fault, twinning occurs and the NW continues to grow with a triangular base, which however points in the opposite $[2\bar{1}\bar{1}]$ direction. The density of these twinned NWs depends somewhat on the detailed growth conditions (the in–depth experimental investigation of this issue is beyond the scope of this paper), but in most samples was as small as 1%.

NWs were also characterized by transmission electron microscopy (TEM); for this purpose they were mechanically transferred on carbon–coated copper grids by gently rubbing the grids on the substrate, and analyzed by means of high–resolution TEM and energy–dispersive x–ray spectroscopy (EDX) in a JEOL 2200FS microscope operating at 200 keV.

Figure 5 shows High Angle Annular Dark Field (HAADF) images of (a) a wire with smooth sidewalls and (b) a wire showing sawtooth faceting, both viewed along the $[2\bar{1}\bar{1}]$ beam direction. The observation of a triangular HAADF intensity profile in $[2\bar{1}\bar{1}]$ zone–axis (see inset in Figure 5a) confirms that the NWs have triangular sections with $\{211\}$–type side facets.

The high–Z catalyst particle is clearly visible in the HAADF images, and is located at the NW tip, which is a distinct characteristic of the tip–based VLS/VSS growth mechanism. A possible correlation between the morphology of the NW facets and the catalyst composition was probed by high resolution TEM (HRTEM) studies and EDX spectroscopy. HRTEM analyses (Figure 6a) reveal that the particle is crystalline, with visible lattice fringes spaced by 0.228 ± 0.005 nm. The Fast Fourier Transform in the inset of Figure 6a shows red spots corresponding to zincblende

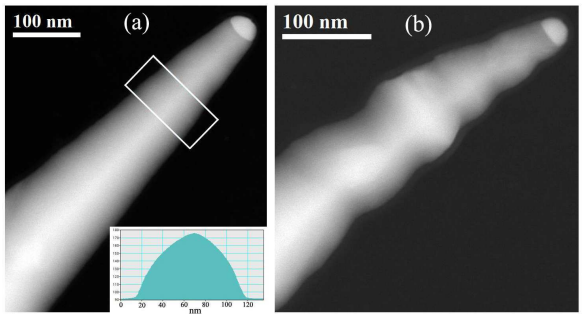

Figure 5: HAADF images of typical wires with (a) smooth and (b) zig–zagged sidewalls, viewed along the $[2\bar{1}\bar{1}]$ beam direction. The inset in (a) shows the intensity profile obtained from the boxed region of the nanowire.

InAs in $[2\bar{1}\bar{1}]$ zone axis and blue spots from the catalyst tip region. Chemical analyses by EDX spectroscopy and mapping (see Figure 6b,c) show that the tip contains Pd and In in a 50:50 ratio, as estimated by the standardless ratio method considering the characteristic Pd L and In L lines, and small traces of Arsenic (<3 at%). Therefore a significant amount of growth material is incorporated into the catalytic particle, which changes the volume and, therefore, the diameter of the particle from its initial value. The spacing of the catalyst lattice fringes in HRTEM images is in good agreement with the value of 0.229 nm expected for $\{110\}$ planes of a body centered cubic PdIn alloy with B2 structure.[28]

As for the PdIn catalyst composition, no variations were detected between NWs with smooth and zig–zagged sidewalls. The issue of Pd incorporation in the InAs lattice was investigated by EDX spectroscopy on different NW segments. Within the sensitivity of this technique, the Pd signal is negligible, and no clusters or precipitates were found in any of the examined NWs. This suggests that the catalyst material is not significantly incorporated into the NWs during growth.

Structural TEM analyses revealed on average a higher defectivity of the NWs with zig–zagged facets compared to those with smooth sidewalls. The occurrence of extended defects is observed, when the NWs are viewed both along $\langle 211\rangle$– and $\langle 110\rangle$–type zone axes. Typical HRTEM micrographs of tapered zig–zagged NW segments in the two projections are shown in Figure 7. Stacking faults on $\{111\}$–type planes, giving the characteristic streaky pattern in the FFT of Figure 7b, are the dominant planar defects.

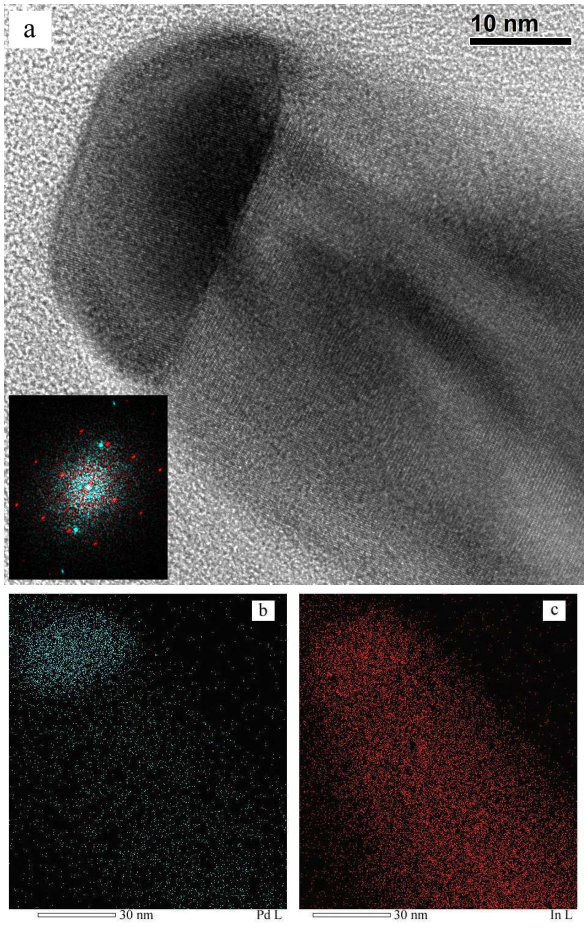

Figure 6: (a) HRTEM image of a NW tip in $[2\bar{1}\bar{1}]$ zone axis. The corresponding FFT, with InAs spots in red and catalyst spots in blue, is shown in the inset. (b) and (c) EDX maps of Pd and In, respectively, obtained considering the characteristic L lines.

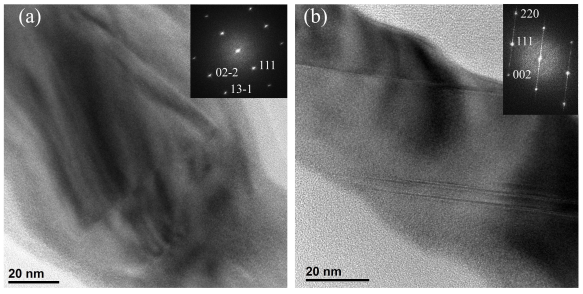

Figure 7: HRTEM images of two NW segments with zig–zagged sidewalls, viewed along the (a) $[2\bar{1}\bar{1}]$ and (b) $[1\bar{1}0]$ beam direction. The corresponding FFTs are shown in the insets.

Strong diffraction contrast effects occur, resulting in considerable variations of the TEM imaging conditions on a local scale. In the zig–zagged NWs, local distortions and slight rotations of the lattice planes can be identified. As a case study of a severe distortion, the near–tip segment of the same NW as reported in Figure 7a was selected. Its HRTEM micrograph in Figure 8 was processed by geometric phase analysis (GPA)[29,30] to gain quantitative information about strain values and its spatial distribution. A relative rotation between adjacent regions of the NW is found: as seen in the rotation map in Figure 8b, as the growth proceeded a rotation by an angle of about 3° on a $\langle 2\bar{1}\bar{1} \rangle$ axis (beam direction for the HRTEM view) occurred. As indicated by the radial (ε_{xx}, Figure 8c) and axial (ε_{yy}, Figure 8d) strain maps, the rotation is accompanied by a significant deformation of $\{0\,1\,1\}$ planes, while the strain of the $(1\,1\,1)$ planes perpendicular to the growth axis is weak or negligible. We note that in NWs with smooth sidewalls, no such rotation or deformation of $\{0\,1\,1\}$ planes were observed (see the Supporting Information for more details).

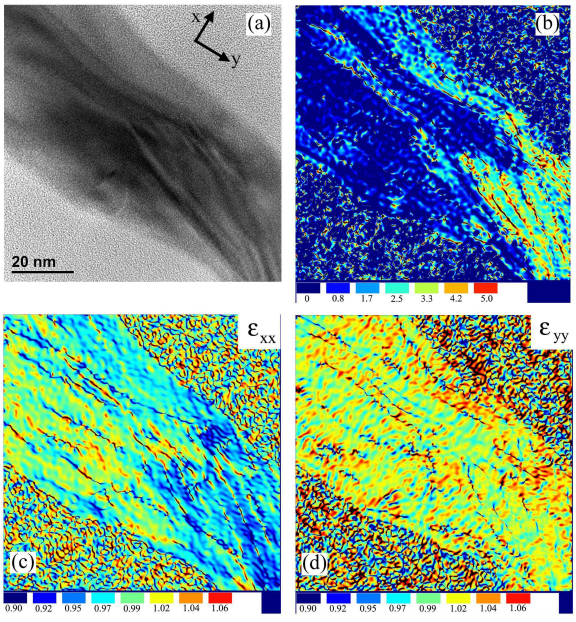

Figure 8: (a) HRTEM image of a NW with zig–zagged sidewalls taken in $[2\bar{1}\bar{1}]$ zone axis. The x and y arrows are along the $[0\,1\,\bar{1}]$ and $[1\,1\,1]$ directions, respectively. (b) Rotation map as obtained by GPA analysis. The angular scale is in degrees. (c),(d) Strain maps. The reference value is set to 1.

A periodic sawtooth surface structure was observed for Si NWs[31] and GaAs NWs[26] and was

attributed to a sawtooth faceting of the NW sidewalls. According to Ross et al.,[31] ideally smooth NW sidewalls can only be expected to grow if allowed facets parallel to the growth direction exist; otherwise steady-state growth can only proceed by a periodic alternation of two stable sidewall facets: as the wire grows wider, the catalyst particle is stretched thinner and meets the NW at a steeper angle. This generates an inward force favoring introduction of the other facet. Conversely, the narrowing of the wire leads to the catalyst particle applying an outward force on the wire, eventually resulting in the introduction of the widening facet.

In fact, according to a model by Zou et al.[26] developed for III-V zincblende NWs, lateral growth along the $\langle 1\,1\,2\rangle$A directions actually takes place on their associated $\{1\,1\,1\}$ planes. A defect in the wire holds back the lateral growth, leaving a terminating $\{0\,0\,2\}$ crystal plane. Finally this results in a V-shaped NW sidewall segment. We believe that a similar mechanism can be applied here. During growth of the InAs NWs in $[1\,1\,1]$A direction, an instability in the $\{1\,1\,2\}$A surfaces parallel to the growth direction leads to faceting of the sidewalls in alternating $\{1\,1\,1\}$ and $\{0\,0\,2\}$ planes.

The model of Ross et al.[31] is based on the VLS growth mode. Therefore we assume that catalyst particles on top of the zig–zag NWs are liquid during growth. According to Ross et al., the period λ and the amplitude ΔR of the sidewall sawtooth oscillations scale with the diameter R of the NW. This poses the question why here we observe a critical diameter d_c above which NW sidewalls are smooth and not faceted. We speculate that the catalyst particle above the critical diameter is solid, and growth proceeds in the VSS mode. This would naturally explain the observation of a bimodal tip–size distribution. Being solid, the catalyst particle cannot change its diameter during growth and therefore forces the NW to grow with smooth sidewalls. The size–dependence of melting temperature in metals is well known,[32] and smaller particles have a lower melting point. Therefore, in a material–dependent temperature range, small liquid and large solid particles can coexist on a surface. Model and experiment report that for increasing temperature, the critical radius for melting increases.[32] This is matching our experimental observation: as shown in Figure 4, we measure a variation of the critical diameter d_c by approximately 20 nm upon a temperature variation of 10 K.

We are not aware of detailed data relative to PdInAs ternary alloys, but the order–of–magnitude variation observed here seems compatible with values reported in literature for In and Au.[32] This is strong circumstantial evidence for our assumption of small liquid and large solid catalyst particles during growth.

PdC16 is a negative–tone direct–write electron resist.[20,33] We patterned PdC16 films after spin–coating on the InAs substrate by electron beam lithography (EBL) before thermolysis. Various patterns were written at 20 kV accelerating voltage with a dose of 2.8 mC/cm^2. The substrate was then developed in toluene for 10 s to remove the unexposed resist. This yielded a patterned film of the Pd nanoparticles, as verified by SEM. As a consequence, growth of InAs NWs occured selectively in the regions of the sample with Pd coverage (e.g., SEM micrograph in Figure 9(a)).

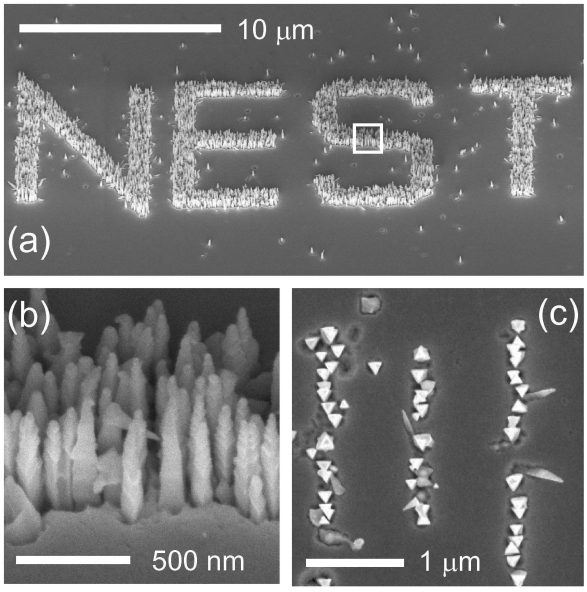

Figure 9: (a) SEM side–view image of Pd–assisted InAs NWs, grown on a patterned substrate, obtained by EBL of the PdC16 film; for the SEM imaging the sample was tilted by 45°. (b) Zoom–in into the region with NWs indicated by the white box in (a). (c) SEM top–view image of lines of single NWs, grown on a patterned PdC16 film.

Figure 9(b) shows a zoom–in into one of the areas with NWs (indicated by the white box in Figure 9(a)) which reveals the same NW morphology as shown before in Figure 2 and Figure 3. However, the NW density is clearly different. This highlights another peculiar feature of the PdC16 precursor: Pd nanoparticle density can be tuned by the PdC16 film thickness prior to thermolysis.

Figure 9(c) finally shows that even single NW lines can be obtained with this method.

In conclusion, we demonstrated the Pd–assisted growth of InAs NWs on InAs$(1\,1\,1)$A surfaces. The wires grow with zincblende structure in the $[1\,1\,1]$A direction. The catalyst particle (composition 50% Pd and 50% In) is located at the tip of the NWs, and Pd is not incorporated into the NWs during growth. NWs show a triangular cross–section with $\{1\,1\,2\}$A sidewall surfaces. Two types of NWs sidewalls are found, smooth and zig–zag, which grow from large and small catalyst particles, respectively. Based on temperature–dependent measurements, we speculate that the small particles are liquid during growth, giving rise to the zig–zagged sidewalls, while the large particles are solid and lead to the growth of NWs with smooth sidewalls. Finally, since PdC16 is a direct–write electron beam resist, the Pd precursor film can be easily patterned. Our results open new routes to applications in microelectronics, molecular electronics, photovoltaics, and for NW–based sensor applications.

Acknowledgement

We acknowledge financial support from Monte dei Paschi di Siena with the project *Implementazione del laboratorio di crescita dedicato alla sintesi di nanofili a semiconduttore*, the bilateral project of Ministero degli Affari Esteri *Nanocharacterization of nanowires, nanomagnets and laser diodes for sensors, optoelectronics and data storage (N3)*, the EU program NODE 015783, FIRB project prot. RBIN067A39_002, and the Indo–Italian POC in S&T 2008 – 2010. RB thanks CSIR for her fellowship.

Supporting Information Available

Additional results: the RHEED data in greater detail; rotation and strain maps for a NW with smooth sidewalls.

This material is available free of charge via the Internet at `http://pubs.acs.org`.

References

(1) Kolasinski, K. W. *Current Opinion in Solid State and Materials Science* **2006**, *10*, 182.

(2) Lu, W.; Lieber, C. M. *J. Phys. D: Appl. Phys.* **2006**, *39*, R387.

(3) Fan, H. J.; Werner, P.; Zacharias, M. *Small* **2006**, *2*, 700.

(4) Dick, K. A. *Progress in Crystal Growth and Characterization of Materials* **2008**, *54*, 138.

(5) Nguyen, P.; Ng, H. T.; Meyyappan, M. *Adv. Mater.* **2005**, *17*, 1773.

(6) Tuan, H.-Y.; Lee, D. C.; Korgel, B. A. *Angew. Chem. Int. Ed.* **2006**, *45*, 5184.

(7) Ford, A. C.; Ho, J. C.; Fan, Z.; Ergen, O.; Altoe, V.; Aloni, S.; Razavi, H.; Javey, A. *Nano Res.* **2008**, *1*, 32.

(8) Ke, Y.; Weng, X.; Redwing, J. M.; Eichfeld, C. M.; Swisher, T. R.; Mohney, S. E.; Habib, Y. M. *Nano Letters* **2009**, *9*, 4494.

(9) Ivey, D. G. *Platinum Metals Rev.* **1999**, *43*, 2.

(10) Lysczek, E. M.; Mohney, S. E.; Wittberg, T. N. *Electronics Letters* **2003**, *39*, 1866.

(11) Lysczek, E. M.; Robinson, J. A.; Mohney, S. E. *Materials Science and Engineering B* **2006**, *134*, 44.

(12) Dormaier, R.; Zhang, Q.; Liu, B.; Chou, Y. C.; Lange, M. D.; Yang, J. M.; Oki, A. K.; Mohney, S. E. *J. Appl. Phys.* **2009**, *105*, 044505.

(13) Seminario, J. M.; De La Cruz, C. E.; Derosa, P. A. *J. Am. Chem. Soc.* **2001**, *123*, 5616.

(14) Springborg, M. *Europhys. Lett.* **1990**, *11*, 325.

(15) Humphrey, D. S.; Cabailh, G.; Pang, C. L.; Muryn, C. A.; Cavill, S. A.; Marchetto, H.; Potenza, A.; Dhesi, S. S.; Thornton, G. *Nano Letters* **2009**, *9*, 155.

(16) Hofmann, S.; Sharma, R.; Wirth, C. T.; Cervantes-Sodi, F.; Ducati, C.; Kasama, T.; Dunin-Borkowski, R. E.; Drucker, J.; Bennett, P.; Robertson, J. *Nature Materials* **2008**, *7*, 372.

(17) Saito, Y.; Nishikubo, K.; Kawabata, K.; Matsumoto, T. *J. Appl. Phys.* **1996**, *80*, 3062.

(18) Takagi, D.; Homma, Y.; Hibino, H.; Suzuki, S.; Kobayashi, Y. *Nano Letters* **2006**, *6*, 2642.

(19) Thomas, P. J.; Lavanya, A.; Sabareesh, V.; Kulkarni, G. U. *Proc. Indian Acad. Sci. (Chem. Sci.)* **2001**, *113*, 611.

(20) Bhuvana, T.; Kulkarni, G. U. *ACS Nano* **2008**, *2*, 457.

(21) Radha, B.; Kulkarni, G. U. *Small* **2009**, *5*, 2271.

(22) Ercolani, D.; Rossi, F.; Li, A.; Roddaro, S.; Grillo, V.; Salviati, G.; Beltram, F.; Sorba, L. *Nanotechnology* **2009**, *20*, 505605.

(23) Wacaser, B. A.; Deppert, K.; Karlsson, L. S.; Samuelson, L.; Seifert, W. *J. Crystal Growth* **2006**, *287*, 504.

(24) Taguchi, A.; Kanisawa, K. *Appl. Surf. Sci.* **2006**, *252*, 5263.

(25) Zhu, J.; Yu, Z.; Burkhard, G. F.; Hsu, C.-M.; Connor, S. T.; Xu, Y.; Wang, Q.; McGehee, M.; Fan, S.; Cui, Y. *Nano Letters* **2009**, *9*, 279.

(26) Zou, J.; Paladugu, M.; Wang, H.; Auchterlonie, G. J.; Guo, Y.-N.; Kim, Y.; Gao, Q.; Joyce, H. J.; Tan, H. H.; Jagadish, C. *Small* **2007**, *3*, 389.

(27) Verheijen, M. A.; Algra, R. E.; Borgström, M. T.; Immink, G.; Sourty, E.; van Enckevort, W. J. P.; Vlieg, E.; Bakkers, E. P. A. M. *Nano Letters* **2007**, *7*, 3051.

(28) Kim, H. S.; Lee, K. H.; Shin, M. C. *Scripta Materialia* **1998**, *38*, 1549.

(29) Hÿtch, M. J.; Snoeck, E.; Kilaas, R. *Ultramicroscopy* **1998**, *74*, 131.

(30) We performed the analysis using the software STEM CELL (http://tem.s3.infm.it/software).

(31) Ross, F. M.; Tersoff, J.; Reuter, M. C. *Phys. Rev. Lett.* **2005**, *95*, 146104.

(32) Couchman, P. R.; Jesser, W. A. *Nature* **1977**, *269*, 481.

(33) Bhuvana, T.; Gregoratti, L.; Heun, S.; Dalmiglio, M.; Kulkarni, G. U. *Langmuir* **2009**, *25*, 1259.

Supporting Information for

Pd–assisted growth of InAs nanowires

Stefan Heun,[*,†] Boya Radha,[‡] Daniele Ercolani,[†] Giridhar U. Kulkarni,[‡] Francesca Rossi,[¶] Vincenzo Grillo,[§] Giancarlo Salviati,[¶] Fabio Beltram,[†] and Lucia Sorba[†]

NEST, CNR–INFM and Scuola Normale Superiore, Piazza S. Silvestro 12, I–56127 Pisa, Italy, Jawaharlal Nehru Centre for Advanced Scientific Research, Jakkur P. O., Bangalore 560 064, India, IMEM–CNR, Parco Area delle Scienze 37/A, I–43010 Parma, Italy, and INFM–CNR National Research Center on nanoStructures and bioSystems at Surfaces (S3), via Campi 213/A, I–41100, Modena (Italy)

E-mail: stefan.heun@sns.it

RHEED analysis

Reflection high energy electron diffraction (RHEED) is a useful tool to study the growth of NW, because the electron beam travels through the NWs, and so the main contribution to the diffraction pattern is due to the three-dimensional volume diffraction inside the NWs. The diffraction geometry is similar to diffraction by TEM.[1] Before the growth of the NWs, the InAs(111)A surface displayed a 2×2 reconstruction in RHEED, in agreement with reports in literature.[2] The RHEED

[*]To whom correspondence should be addressed
[†]NEST, CNR–INFM and Scuola Normale Superiore, Piazza S. Silvestro 12, I–56127 Pisa, Italy
[‡]Jawaharlal Nehru Centre for Advanced Scientific Research, Jakkur P. O., Bangalore 560 064, India
[¶]IMEM–CNR, Parco Area delle Scienze 37/A, I–43010 Parma, Italy
[§]INFM–CNR National Research Center on nanoStructures and bioSystems at Surfaces (S3), via Campi 213/A, I–41100, Modena (Italy)

patterns observed after NW growth are shown in Figure 1 (a)–(c). (a) was measured with the electron beam in the $[10\bar{1}]$ substrate direction. Equivalent diffraction patterns were measured in the $[\bar{1}10]$ and $[0\bar{1}1]$ directions, which can be reached from the $[10\bar{1}]$ direction by an in-plane rotation of $\pm 120^\circ$. A similar pattern, but tilted in the opposite direction, was obtained in the $[01\bar{1}]$ direction and is shown in Figure 1(c). The $[10\bar{1}]$ and the $[01\bar{1}]$ directions are both in the (111)A plane and include an angle of 60°. Equivalent diffraction patterns as the one shown in (c) were measured in the $[\bar{1}01]$ and the $[1\bar{1}0]$ directions, which can be obtained from the $[01\bar{1}]$ direction by an in-plane rotation of $\pm 120^\circ$. Therefore, for each in-plane rotation by 60° the diffraction pattern changes from (a) to (c) and back to (a) etc. For all intermediate 30° rotations, a diffraction pattern as the one shown in Figure 1(b) was observed. The displayed pattern was measured in the $[11\bar{2}]$ direction, which is in between the $[10\bar{1}]$ and the $[01\bar{1}]$ directions. For all directions the RHEED pattern shows well-defined spots, which indicates that the majority of NWs have the same crystalline structure and orientation.

The experimentally observed patterns were compared to computed diffraction patterns, using the EMS On Line site (http://cecm.insa-lyon.fr/CIOLS/crystal1.pl). Simulations were performed for an acceleration voltage of 12 kV and a camera distance of 500 mm, corresponding to the parameters in the experiment. We have computed diffraction patterns for zincblende (Figure 1 (d)–(f)) and wurtzite structures (Figure 1 (g)–(i)) for comparison. For the zincblende calculations it was assumed that the NWs grow in the $[111]$A direction. Diffraction patterns for the $[10\bar{1}]$, $[11\bar{2}]$, and $[01\bar{1}]$ directions are shown in Figure 1 (d), (e), and (f), respectively. For comparison with the experimental RHEED data the computed maps were rotated so that the $[111]$A direction points downwards in the figure. The calculated RHEED patterns show good qualitative agreement with the measured diffraction patterns.

Another crystal structure often observed for the growth of III-V NWs on (111) surfaces is wurtzite.[1] In this case, the NWs grow with their $[001]$ direction normal to the (111) surface, and the directions corresponding to the above mentioned substrate directions are the $[\bar{1}20]$, $[\bar{1}10]$, and $[\bar{2}10]$ directions of the NW wurtzite crystal.[3] Corresponding calculated diffraction patterns are

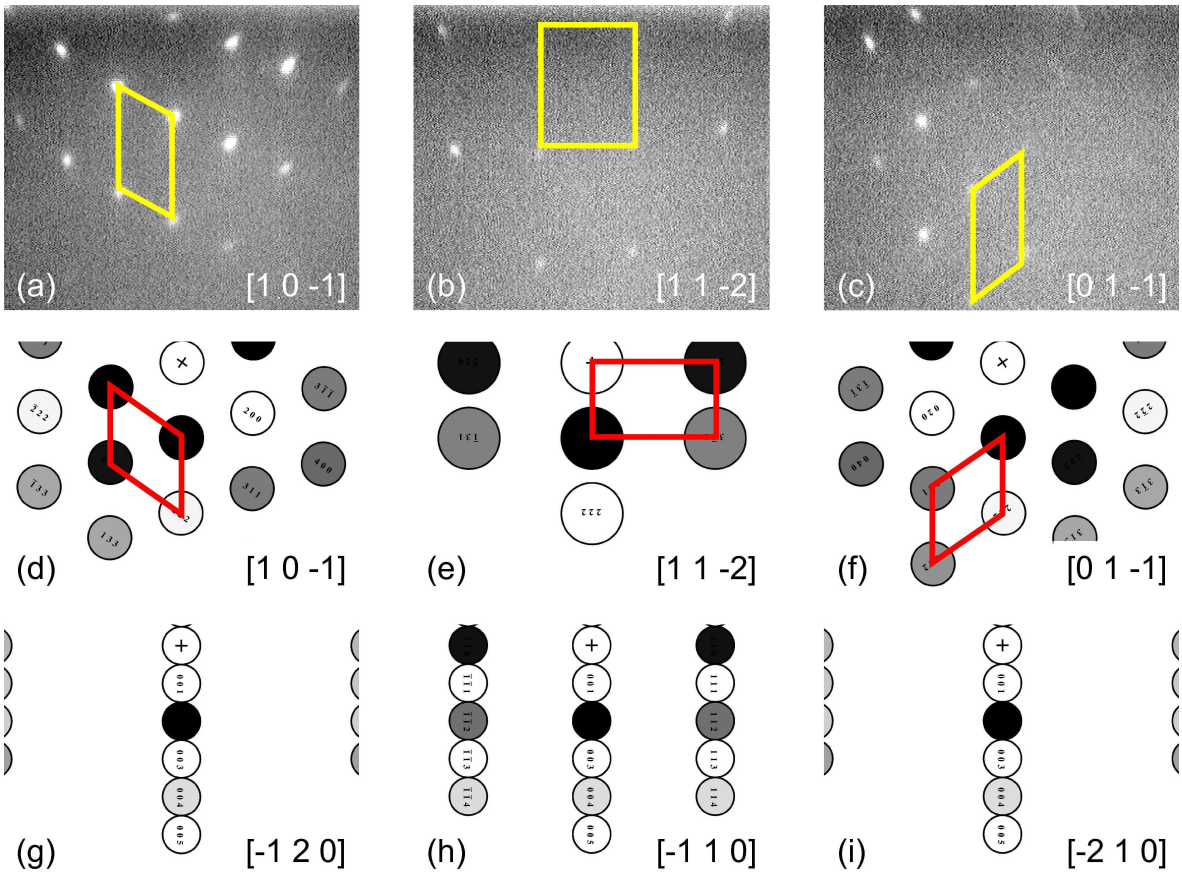

Figure 1: (a)–(c): Experimentally observed RHEED patterns for the directions indicated in each figure. The drawn parallelograms indicate the geometric arrangement of the diffraction spots. (d)–(f): Calculated diffraction patterns for zincblende NWs growing in the [111]A direction. The azimuthal orientation is as in (a)–(c). Good agreement to experiment is observed. (g)–(i): The same as (d)–(f), assuming wurtzite NWs growing in the [100] direction. These patterns are clearly not compatible with experiment.

shown in Figure 1 (g), (h), and (i), respectively. The calculated patterns were oriented so that their [001] direction points downwards in the figure. As can be seen, the patterns show no resemblance with the experimentally observed ones, and in particular, if the NWs would grow with a wurtzite structure, the diffraction patterns for the $[\bar{1}20]$ and $[\bar{2}10]$ directions should be equal, which is clearly not the case. This discards the possibility that the NWs grow with a wurtzite structure and adds further evidence to the supposition of epitaxial growth of the NWs in [111]A direction with zincblende structure.

GPA analysis for NWs with smooth sidewalls

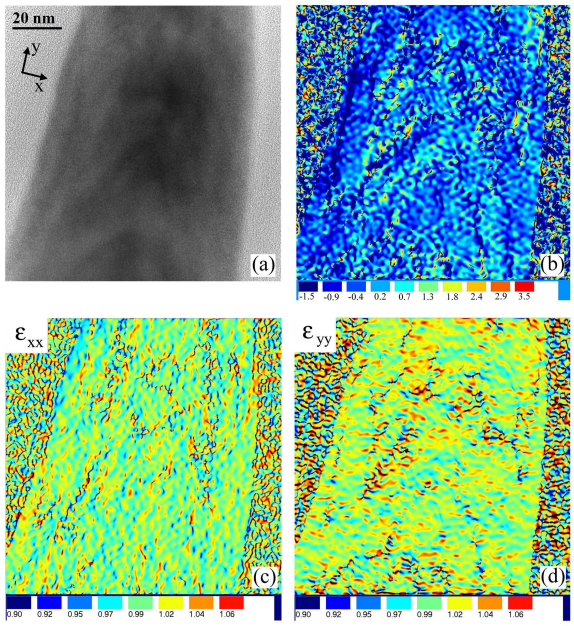

Figure 2: GPA analysis on a NW with smooth sidewalls. (a) HRTEM image taken in $[2\bar{1}\bar{1}]$ zone axis. The x and y arrows are along the $[01\bar{1}]$ and [111] directions, respectively. (b) Rotation map; the angular scale is in degrees. (c),(d) Strain maps. The reference value is set to 1.

References

(1) Tchernycheva, M.; Harmand, J. C.; Patriarche, G.; Travers, L.; Cirlin, G. E. *Nanotechnology* **2006**, *17*, 4025.

(2) Taguchi, A.; Kanisawa, K. *Appl. Surf. Sci.* **2006**, *252*, 5263.

(3) Verheijen, M. A.; Algra, R. E.; Borgström, M. T.; Immink, G.; Sourty, E.; van Enckevort, W. J. P.; Vlieg, E.; Bakkers, E. P. A. M. *Nano Letters* **2007**, *7*, 3051.